# Strongly hybridized dipole-exchange spin waves in thin Fe-N ferromagnetic films

Silvia Tacchi,[1,*] Raffaele Silvani,[2] Giovanni Carlotti,[2] Massimiliano Marangolo,[3] Mahmoud Eddrief,[3] Angelo Rettori,[4] and Maria Gloria Pini[5]

[1]*Istituto Officina dei Materiali del CNR (CNR-IOM), Sede Secondaria di Perugia, c/o Dipartimento di Fisica e Geologia, Università di Perugia, I-06123 Perugia, Italy*

[2]*Dipartimento di Fisica e Geologia, Università di Perugia, I-06123 Perugia, Italy*

[3]*Sorbonne Université, CNRS, Institut des NanoSciences de Paris, INSP, UMR 7588, F-75005 Paris, France*

[4]*Dipartimento di Fisica ed Astronomia, Università di Firenze, I-50019 Sesto Fiorentino, Italy*

[5]*Istituto dei Sistemi Complessi del CNR (CNR-ISC), Sede Secondaria di Firenze, I-50019 Sesto Fiorentino, Italy*

(Received 6 June 2019; revised manuscript received 25 July 2019; published 3 September 2019)

Spin waves propagation in ferromagnetic films, several tens of nanometers thick, have recently received increasing attention, in view of the development of magnonic devices operating in the GHz range of frequencies. A detailed knowledge of the dispersion curves and of the spatial characteristics of the spin-wave modes is preliminary to any technological application, particularly in the "mesoscopic range" (50–200 nm) of film thickness, where several dipole-exchange modes may appear in the spectrum, exhibiting frequency crossing and hybridization as a function of their wave number. In this work, the mutual interaction and the hybridization of the dipole-exchange spin-wave modes was investigated in a nitrogen-implanted iron (Fe-N) film, 78-nm-thick, in-plane magnetized. The spin-wave dispersion curves were measured by using Brillouin light scattering, and the experimental results were interpreted combining micromagnetic simulations and theoretical calculations in the framework of a dipole-exchange spin-wave mode approach. A noticeable hybridization between the spin-wave modes was observed, due to the simultaneous presence of a marked perpendicular magnetic anisotropy and a rather high saturation magnetization. The hybridization was found to induce a very large gap ($\Delta\nu \approx 5$ GHz) between the low-frequency spin waves at high wave vector ($k \approx 10^5$ rad/cm). Consequently, in such a $k$ range the simultaneous presence of two spin-wave modes with sizeable ($v_g \approx 1.5$ km/s) but opposite group velocity was observed, opening a way for the potential use of Fe-N films in magnon spintronics.

DOI: 10.1103/PhysRevB.100.104406

## I. INTRODUCTION

Spin-wave (SW) states, introduced by Felix Bloch in 1930, are the lowest-lying excited levels of an ordered ferromagnet, and thus the most important ones from the thermodynamics point of view. In spite of this long period of time, during which the spin dynamics was investigated in a variety of magnetically ordered systems [1], a revival in the study of spin waves took place in recent years because research fields, such as magnon spintronics [2–5], emerged at the border between spin dynamics and nanoscale devices. In this context, spin waves can be used to carry and process information, with the perspective of avoiding ohmic losses and preventing energy dissipation. Historically, applications in telecommunication systems and radars [6] were concerned with spin waves in the GHz range of frequencies, propagating in several $\mu$m thick films of low-dissipating materials, such as Yttrium Iron Garnet (YIG). Similar films were also exploited more recently to achieve the Bose-Einstein condensation of magnons at room temperature [7,8]. In such relatively thick films, the SW spectrum is quasicontinuum, given the large number of guided modes; nevertheless, one can put in evidence the so-called Damon-Eshbach (DE) surface mode, when the magnetostatic surface spin-wave (MSSW) geometry (film magnetized in-plane and SW wave vector orthogonal to the magnetization) is exploited [5]. If the film thickness is reduced below 20–30 nm, on the other hand, only one mode is observed at GHz frequencies, still named the DE mode in the MSSW geometry, characterized by a rather uniform spatial profile across the film thickness. This is because the rich spectrum of perpendicularly standing spin waves (PSSW) is lifted to much higher frequencies, due to the vertical confinements effect and the consequent cost, in terms of exchange energy, of one or more nodes across the film thickness. For instance, a recent study of the propagation of the DE mode in a 30- nm-thick YIG film [9] demonstrated a strong protection against backscattering from surface defects, in a wide range of wave vectors ($0 < k < 10^6$ rad/cm), where its frequency lies inside the gap of the PSSW modes. It is notable that this protection is a consequence of the breaking of time-reversal symmetry due to off-diagonal terms in the dipolar interaction tensor. For film thickness in the "mesoscopic range" between about 50 and a few hundreds of nanometers, instead, the SW spectrum can be rather complex, since it consists of several discrete modes in the range between 1 and 30 GHz. These modes result from the mixing and the hybridization of the DE and PSSW modes, and they have attracted considerable interest both in

*tacchi@iom.cnr.it

 

the context of metallic films [10,11] and of YIG/metallic layer heterostructures [12,13]. All these studies put in evidence that, in the current effort to design high-frequency devices, it can be important to achieve efficient excitation of high-order discrete modes in films with "mesoscopic thickness", where the hybridization of the DE mode with one or more PSSW modes allows one to operate at much higher frequency with respect to the case of the ordinary DE mode of thin films. In this respect, it has been found that relevant SW properties are significantly affected by the strong hybridization between PSSW and DE modes [11,14]. In particular, an enhancement of the group velocity of both the DE and the PSSW modes has been observed [13].

Therefore, a detailed knowledge of the SW spectrum is mandatory to design highly efficient magnonic devices.

In this paper, we present an accurate study of the lowest SW modes propagating in the MSSW geometry in an in-plane magnetized nitrogen-implanted iron thin film (Fe-N) [15], 78-nm thick. This material represents a very suitable system to investigate the SW modes interaction, because its marked perpendicular magnetic anisotropy, combined with a rather high saturation magnetization, results in quite large off-diagonal terms of the dipolar interaction tensor. In previous papers [16,17], some of us have investigated the magnetization configuration and the ferromagnetic resonance (corresponding to SW's with zero wave vector) of such a film, which presents a 100-nm-periodic magnetic stripe domain structure [18] for sufficiently low intensities of an in-plane applied magnetic field. Here, instead, we report an accurate study of the lowest SW modes of a Fe-N film, 78-nm thick, in the presence of a saturating magnetic field applied in plane, but perpendicular to the SW propagation direction (MSSW geometry).

The SW dispersion relation has been measured by Brillouin light scattering (BLS) and compared to micromagnetic simulations, based on a graphic processing unit (GPU)-accelerated software [19]. The agreement was very good and we were able to account not only for the dependence of the frequency on the SW propagation wave vector, but also for the marked asymmetry between Stokes and anti-Stokes sides of the BLS spectra, which reflects the intrinsic nonreciprocity of some of the modes. Moreover, theoretical calculations have been performed solving the linearized Landau-Lifshitz equations of motion in the framework of the spin-wave mode approach [20–24]. By this method, the exact dispersion relation for dipole-exchange spin waves is expressed in terms of a vanishing infinite determinant and an infinite convergent series. Hence, the eigenvalues and eigenvectors can be obtained to various degrees of approximation. This has allowed us to illustrate the spatial profiles of the spin-wave modes and to understand the important role played by the competition between short-range exchange coupling, long-range magnetic dipole-dipole interactions and perpendicular magnetic anisotropy in the Fe-N thin film. In particular, a strong hybridization between the dipole-exchange spin-wave modes, produced by the off-diagonal parts of the dipolar interaction tensor, has been observed for in-plane wave vectors $k$ larger than about $10^5$ rad/cm. Noticeably, the hybridization was found to induce a very large gap ($\Delta\nu \approx 5$ GHz) between the frequencies of the spin-wave modes at high wave vector ($k \approx 10^5$ rad/cm), in agreement with the experiment.

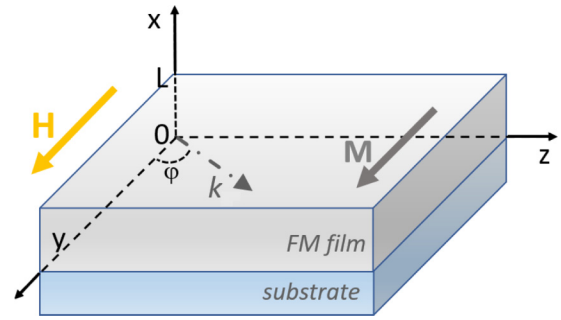


FIG. 1. The reference frame. The ferromagnetic film has finite thickness $L$ in the $x$ direction. A saturating magnetic field **H** is applied in plane along the $y$ direction. The in-plane propagation wave vector of the spin wave **k** forms an angle $\varphi$ with the equilibrium magnetization **M**. In the experiments, the MSSW configuration, corresponding to $\varphi = 90^\circ$, was exploited.

## II. EXPERIMENT AND MICROMAGNETIC MODELING

An $\alpha$-Fe film, with thickness $L = 78$ nm, has been deposited by molecular beam epitaxy on a ZnSe/GaAs (001) substrate, and protected against oxidation by an 8-nm-thick gold capping layer. Reflection high-energy electron diffraction measurements indicated that the [110] ([100]) axis of $\alpha$-Fe, ZnSe, and GaAs were parallel to each other. Ion implantation was performed at room temperature with nitrogen molecular ions $N^{+2}$ accelerated to 40 keV with a fluence of $5.3 \times 10^{16}$ ions/cm$^2$. The ion current density was kept below 3 $\mu$A/cm$^2$ and the targets were not cooled during implantation. The crystal structure of the sample was studied by means of x-ray diffraction measurements in the out-of-plane direction using monochromatized Cu K$\alpha$ radiation in a high-resolution SmartLab diffractometer. More details about implantation and structural studies are given in [16] and in [25]. The formation of a body-centered tetragonal N martensite, with the $c$ axis perpendicular to the film plane and the $c$ parameter close to that of $\alpha'$-Fe8N, has been observed. BLS measurements were performed in the backscattering configuration, focusing about 200 mW of monochromatic light (wavelength $\lambda = 532$ nm) onto the sample surface. The scattered light was frequency analyzed by a Sandercock-type 3 + 3-pass tandem Fabry-Perot interferometer [26,27]. The SW dispersion relation was measured in the MSSW configuration, applying the external magnetic field parallel to the $y$ axis, and sweeping the in-plane wave vector along the perpendicular direction (i.e., $\varphi = 90^\circ$ in Fig. 1). Because of the conservation of the in-plane momentum in the scattering process, the wave-vector magnitude $k$ is linked to the incidence angle of light $\theta_I$ by the simple relation $k = (4\pi/\lambda)\sin\theta_I$. The intensity of the magnetic field was fixed to $H = 4$kOe to ensure the in-plane saturation of the sample, while the wave vector $k$ was swept in the range between 0 and $2 \times 10^5$ rad/cm.

Micromagnetic simulations have been performed using the GPU-accelerated software [19] MuMax3. The simulated material parameters were set to the following values obtained by previous investigations [15–18]: saturation magnetization $M_s = 1700$ emu/cm$^3$, exchange constant $A_{ex} = 1.8 \times 10^{-6}$ erg/cm, out-of-plane anisotropy constant $K_u = 4.9 \times 10^6$ erg/cm$^3$. The Gilbert damping parameter was set

to $\alpha = 0.001$. To calculate the dependence of the modes frequencies for different values of the wave vector, a stripe geometry was considered, with a length of 6.72 $\mu$m (along $z$), a width of 20 nm (along $y$) and a thickness of 78 nm, discretized in $2048 \times 2 \times 32$ cells, respectively, and in-plane periodic boundary conditions were applied. In order to excite spin waves, a sinc-shaped field pulse $b(t) = b_0 \frac{\sin[2\pi f_0(t-t_0)]}{[2\pi f_0(t-t_0)]}$, directed perpendicularly to the sample plane, with amplitude $b_0 = 100$ Oe and frequency $f_0 = 45$ GHz, was applied in the center of the simulated area in a region having a size of 20 and 105 nm along the $z$ and $y$ directions, respectively. To mimic the limited penetration depth of light into the Fe-N film in the BLS experiments, the dispersion relation was calculated by performing a Fourier transform of the out-of-plane component of the magnetization both in space and time, considering only those simulation cells located in the top 20-nm layer.

## III. DIPOLE-EXCHANGE SPIN-WAVE THEORY

A theory of dipole-exchange spin waves propagating in plane in a tangentially magnetized thin ferromagnetic film [20–24] has been applied to calculate both the dispersion curves and the spatial profiles of the spin-wave modes. The film, see Fig. 1, is supposed to have a finite thickness $L$ in the $x$ direction, and to be infinite in the $yz$ plane. A saturating dc magnetic field $\mathbf{H} = H\mathbf{e}_y$ is applied in the film plane in the positive direction of the $y$ axis, so that the equilibrium magnetization is $\mathbf{M} = M_s\mathbf{e}_y$ (where $M_s$ is the saturation magnetization). The uniaxial magnetic anisotropy $K_u$ favors the out-of-plane (OOP) direction $x$. The in-plane (IP) axis $z$ coincides with the direction of the positive wave vector $k$ of a plane spin wave in the MSSW configuration ($\varphi = 90°$). The magnetization dynamics are described by the linearized Landau-Lifshitz equations of motion [20]

$$\frac{\partial \mathbf{m}}{\partial t} = \gamma[\mathbf{M} \times \mathbf{h}^{\text{eff}} + \mathbf{m} \times \mathbf{H}^{\text{eff}}], \tag{1}$$

where $\mathbf{m}(t)$ is the dynamic magnetization vector, perpendicular to the static magnetization vector $\mathbf{M} = M_s\mathbf{e}_y$, and having cartesian components $m^x$ (the OOP component) and $m^z$ (the IP one). The dynamic effective field $\mathbf{h}^{\text{eff}} = \mathbf{h}_d + \mathbf{h}_{ex} + \mathbf{h}_a$ is the sum of the variable dipolar field, exchange field, and crystallographic anisotropy field, respectively. The static effective field $\mathbf{H}^{\text{eff}} = \mathbf{H} + \mathbf{H}_d + \mathbf{H}_a$ is the sum of the external dc applied field, a constant dipolar field and a constant field of crystallographic anisotropy.

The equations of motion for the magnetization (1) are solved simultaneously with the Maxwell's equations of magnetostatics using the Green's function technique [20–24]. The solution to Eq. (1) is searched for in the form of a Fourier expansion in plane waves [22,24]

$$\mathbf{m}(\mathbf{r}, t) = \sum_k \mathbf{m}_k(x, t)e^{-i\mathbf{k}\cdot\mathbf{r}} + c.c., \tag{2}$$

where $\mathbf{r} = (y, z)$ and $\mathbf{k} = k(\cos\varphi, \sin\varphi)$, see Fig. 1. The coefficients of the expansion, nonuniform across the film thickness, are expressed as [22,24]

$$\mathbf{m}_k(x, t) = \sum_{n,p} m_{nk}^{(p)}(t)\mathbf{S}_n^{(p)}(x), \tag{3}$$

where the spin-wave modes $\mathbf{S}_n^{(p)}(x)$ ($p = 1, 2$) are orthogonal in the interval $0 < x < L$ and satisfy the exchange boundary conditions [22,24]. In the case of totally unpinned surface spins ($\partial\mathbf{m}/\partial x|_{(x=0,L)} = 0$), one has [22,24]

$$\mathbf{S}_n^{(1,2)}(x) = (\mathbf{e}_x \pm \mathbf{e}_z)\frac{1}{\sqrt{1+\delta_{0n}}}\cos\left(\frac{n\pi x}{L}\right) \quad n = 0, 1, 2, \cdots. \tag{4}$$

In this way, the Landau-Lifshitz equations of motion (1) are converted [22] in a system of equations for the spin-wave amplitudes $m_{nk}^{(p)}(t) = e^{i\omega t}m_{nk}^{(p)}$

$$\frac{\partial}{\partial t}m_{n'k}^{(1)} + ia_{n'k}m_{n'k}^{(1)} + ibm_{n'k}^{(2)} + i\sum_n \left[m_{nk}^{(1)}C_{nn'} + m_{nk}^{(2)}(p_{nn'} + q_{nn'})\right] = 0, \tag{5}$$

$$\frac{\partial}{\partial t}m_{n'k}^{(2)} - ib^*m_{n'k}^{(1)} - ia_{n'k}m_{n'k}^{(2)} - i\sum_n \left[m_{nk}^{(1)}(p_{nn'}^* - q_{nn'}^*) + m_{nk}^{(2)}C_{nn'}\right] = 0. \tag{6}$$

The first two coefficients of the spin-wave amplitudes in Eqs. (5) and (6) take the form [22] $a_{nk} = \Omega_{nk} + \frac{\omega_M}{2} - \frac{\omega_U}{2}$ and $b = \frac{\omega_M}{2} - \frac{\omega_U}{2}$, where one has defined the circular frequencies $\Omega_{nk} = \omega_H + \omega_M\alpha[k^2 + (\frac{n\pi}{L})^2]$, $\omega_H = \gamma H$, $\omega_M = \gamma 4\pi M_s$, and $\omega_U = \gamma\frac{2K_u}{M_s}$. The exchange parameter $\alpha = l_{ex}^2$ is the square of the exchange length $l_{ex} = \sqrt{A_{ex}/K_d}$, where $A_{ex}$ is the exchange energy per unit length and $K_d = 2\pi M_s^2$ is the dipolar energy per unit volume. $H$ is the intensity of the external dc bias field, $4\pi M_s$ is the static dipolar field, and $2K_u/M_s$ is an effective static field associated with the out-of-plane magnetic anisotropy, favoring the $x$ direction. The other three coefficients in Eqs. (5) and (6) take the form

$$C_{nn'} = -\frac{\omega_M}{2}(1 - \sin^2\varphi)P_{nn'},$$
$$p_{nn'} = -\frac{\omega_M}{2}(1 + \sin^2\varphi)P_{nn'}, \quad q_{nn'} = -2\omega_M \sin\varphi\, Q_{nn'}. \tag{7}$$

In the case of unpinned surface spins, the explicit expressions [21] for the dimensionless dipolar factors $P_{nn'}$ and $Q_{nn'}$ ($n, n' = 0, 1, 2, \cdots$) are given in Appendix A. They have the following properties: $P_{n'n} = P_{nn'}$ and $Q_{n'n} = -Q_{nn'}$. Moreover, it can be shown that $P_{n,n'} = 0$ if $n$ is even but $n'$ is odd (or *vice versa*); whereas, one has $Q_{n,n'} = 0$ if both $n$ and $n'$ are even (or both odd). The infinite system of equations (5) (6) can be rewritten in matrix form

$$\omega|\mathbf{m}_k\rangle = C_k|\mathbf{m}_k\rangle, \tag{8}$$

where the column vector $|\mathbf{m}_k\rangle$ contains all the spin-wave amplitudes $(m_{0k}^{(1)}, m_{0k}^{(2)}, m_{1k}^{(1)}, m_{1k}^{(2)}, m_{2k}^{(1)}, m_{2k}^{(2)}, \cdots)$ and the square infinite matrix $C_k$ contains all the coefficients of the spin-wave amplitudes in the system of Eqs. (5) and (6).

Explicitly, $C_k$ takes the peculiar block form

$$C_k = \begin{pmatrix} -(a_{0k}+C_{00}) & -(b+p_{00}) & 0 & -q_{10} & -C_{20} & -p_{20} & \cdots \\ (b+p_{00}) & (a_{0k}+C_{00}) & -q_{10} & 0 & p_{20} & C_{20} & \cdots \\ 0 & -q_{01} & -(a_{1k}+C_{11}) & -(b+p_{11}) & 0 & -q_{21} & \cdots \\ -q_{01} & 0 & (b+p_{11}) & (a_{1k}+C_{11}) & -q_{21} & 0 & \cdots \\ -C_{02} & -p_{02} & 0 & -q_{12} & -(a_{2k}+C_{22}) & -(b+p_{22}) & \cdots \\ p_{02} & C_{02} & -q_{12} & 0 & (b+p_{22}) & (a_{2k}+C_{22}) & \cdots \\ \cdots & \cdots & \cdots & \cdots & \cdots & \cdots & \cdots \end{pmatrix}. \quad (9)$$

The eigenvalues of $C_k$ provide the angular frequencies of the dipole-exchange spin-wave modes, while the eigenvectors provide the spin-wave amplitudes. Note that the eigenvalues occur in pairs of opposite sign, corresponding to spin waves propagating in opposite directions [28]. It is fundamental to observe that the hybridization between different spin-wave modes is taken into account through the matrix elements containing the off-diagonal dipole factors: namely, $P_{nn'}$ and $Q_{nn'}$ with $n \neq n'$.

In general, within this theoretical approach [20–24], the problem of determining the whole spectrum of the eigenvalues of the *infinite* matrix $C_k$ cannot be solved exactly. To this regard, it is worth citing an alternative approach [29] which allows the exact calculation of all the spin-wave eigenfrequencies of a layered magnetic structure through the *numerical* solution of a *finite* system of linear equations. Note, however, that from Eq. (9) an approximate *analytical* expression can be obtained setting to zero all the off-diagonal blocks in the *infinite* matrix $C_k$: namely, setting $P_{nn'} = 0$ and $Q_{nn'} = 0$ with $n \neq n'$. Physically, this is equivalent to neglecting any hybridization between different spin-wave modes. In this way, the angular frequencies of the independent dipole-exchange spin-wave modes take the simple analytic form [20–24]

$$\omega_{nk}^2 = [\Omega_{nk} + \omega_M(1 - P_{nn}) - \omega_U][\Omega_{nk} + \omega_M P_{nn} \sin^2\varphi] \quad (n = 0, 1, 2, \cdots). \quad (10)$$

In Appendix B, the influence of both the exchange and the perpendicular anisotropy on the dispersion of the independent spin-wave modes (Fig. 7) has been discussed.

Using the analytical expression (10) for independent modes, the frequency of the DE surface mode and of the perpendicular standing spin-wave modes ($n$-PSSW) characterized by $n$ nodes of the magnetization oscillation through the film thickness, can be obtained for $n = 0$ and $n \neq 0$, respectively. In contrast, setting $P_{nn'} \neq 0$ and $Q_{nn'} \neq 0$ with $n \neq n'$, the hybridization between a finite number of spin-wave modes (the ones with lower energies in the spectrum) can approximately be taken into account [20–24] by numerically calculating the eigenvalues of a *finite* square submatrix of $C_k$. We have checked that, for Fe films in the thickness range where dipole-exchange spin-wave theory holds, the lowest-frequency spin-wave modes numerically calculated through the method [20–24] agree very well with the exact results provided by Hillebrands' method [29].

## IV. RESULTS AND DISCUSSION

Figure 2 reports a sequence of BLS spectra taken for different values of the incidence angle of light (corresponding to different values of the wave vector $k$) applying an in-plane magnetic field $H = 4$ kOe. Note that the peaks appearing in the Stokes or anti-Stokes side, and corresponding to spin waves propagating in opposite directions [28], are rather different. In particular, there is an intense peak on the anti-Stokes side, tagged by an asterisk, that corresponds to a much less intense peak on the Stokes side. Its frequency increases with the wave number, as expected for a DE surface mode. In contrast, the peak that lies at the lowest frequency for most of the $k$ values corresponds to the 1-PSSW mode, as it will

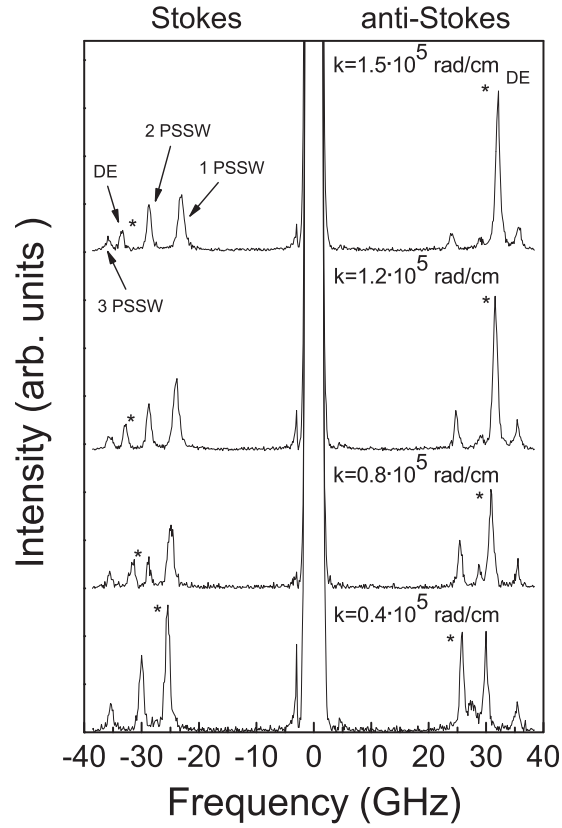


FIG. 2. Brillouin light scattering (BLS) spectra taken for different values of the in-plane transferred wave vector $k$ applying an in-plane magnetic field $H = 4$ kOe. The asterisk marks the surface DE mode.

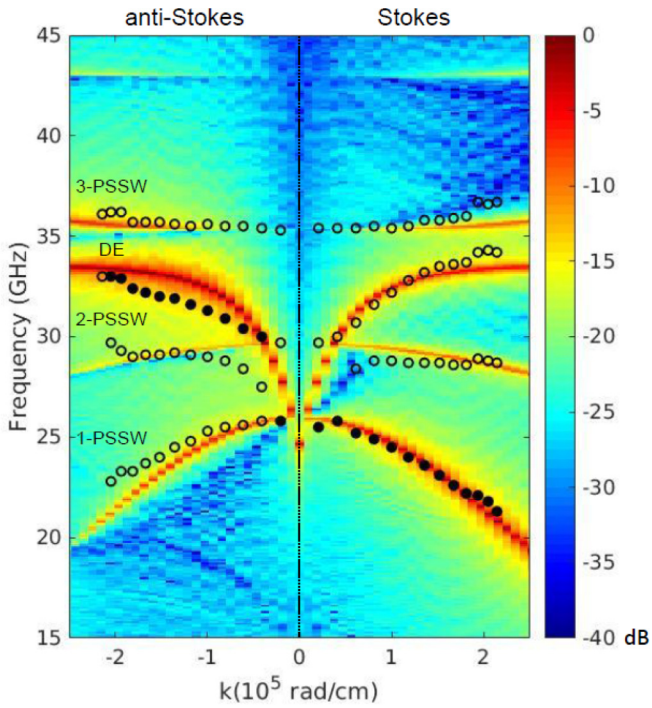


FIG. 3. Comparison between the BLS measured (dots) and the simulated (color plot) frequencies plotted in a log scale as a function of the wave vector $k$. Full dots indicate the most intense peak on each side of the measured spectra. The amplitude of the simulated modes, normalized to the maximum amplitude, is plotted in a log scale. The intensity of the in-plane applied magnetic field is $H = 4$ kOe.

be clarified later on. This mode has the larger intensity on the Stokes side and exhibits an opposite frequency evolution with the wave vector if compared to the DE mode. The other two peaks, labeled 2-PSSW and 3-PSSW, whose spatial profiles will also be analyzed further on, correspond to modes characterized by an almost dispersionless behavior, and have a slightly larger intensity on the Stokes and anti-Stokes side, respectively.

In Fig 3, the measured (dots) evolution of the frequencies with the wave vector is compared with the results of micromagnetic simulations (color plot). It can be seen that not only the measured frequencies are well reproduced in the simulations, but also the intensity of the calculated curves agrees quite well with the relative intensity of the measured peaks in BLS spectra. In particular, for positive (negative) values of $k$, corresponding to the Stokes (anti-Stokes) side of the experimental spectra, the 1-PSSW (DE) mode is always the most intense peak. The 2-PSSW and 3-PSSW modes have a very small intensity for low values of $k$, while they become more intense on increasing $k$. In addition, one can note that the DE mode at zero wave vector starts at a frequency close to the 1-PSSW one; however, while the DE mode exhibits a large positive frequency dispersion and group velocity, the 1-PSSW has a negative frequency evolution with $k$. In addition, a crossing between the DE and the 1-PSSW (at about $0.6 \times 10^4$ rad/cm) and the 2-PSSW (at about $3.5 \times 10^4$ rad/cm) is clearly observed in both the experiment and the simulations.

In order to gain better insight into the above-discussed characteristics of the modes, we exploited the

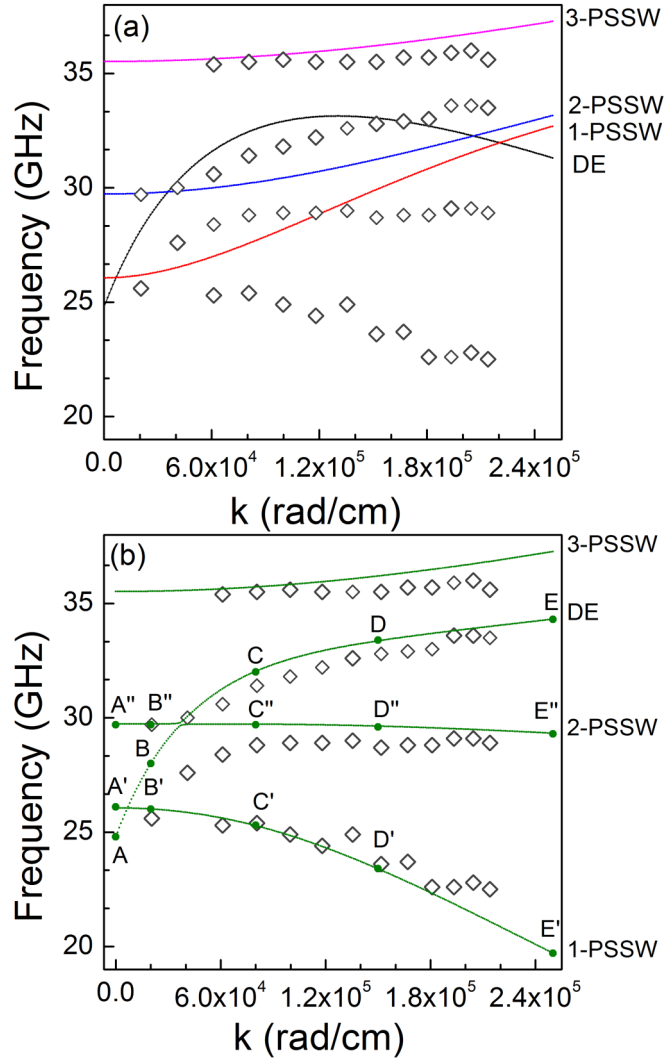


FIG. 4. Comparison between the experimental data (open symbols) and the theoretical frequencies (continuous lines) calculated (a) using the independent dipole-exchange spin-wave model and (b) taking into account the hybridization between the three lowest spin-wave modes. The experimental frequencies are the average of the measured Stokes and anti-Stokes values. The intensity of the in-plane applied magnetic field is $H = 4$ kOe.

dipole-exchange spin-wave theory to calculate both the spin-wave dispersion relations and the spatial profiles, across the film thickness, of the dynamic magnetization components for the various SW modes. The magnetic parameters used in the calculations were the same as in the micromagnetic simulations.

In Fig. 4(a), the BLS measurements are compared with the dispersion relations of the four lowest-lying independent modes, calculated using the approximate analytic expression [Eq. (10) or, equivalently, Eq. (B1) in Appendix B] [20–24]. One can clearly see that, with the exception of the 3-PSSW mode, the independent mode approach is not able to reproduce the experimental results. In fact, especially for large wave-vector values, the calculated dispersion presents a crossing between the DE mode and the 1-PSSW and the 2-PSSW ones, which has not been observed in the BLS data.

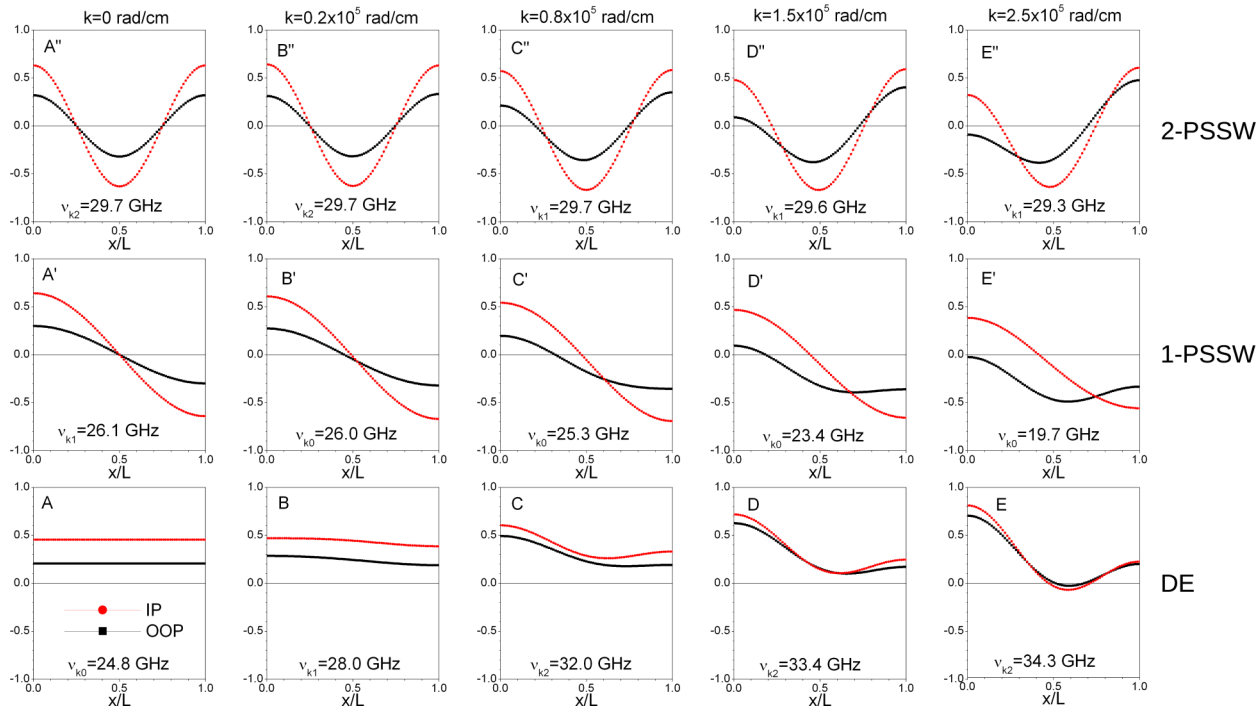


FIG. 5. The distribution of the two dynamic magnetization components, namely the out-of-plane one $m_k^x(x)$ (OOP, black line) and the in-plane one $m_k^z(x)$ (IP, red line), across the film thickness ($0 < x/L < 1$), for the various points denoted by capital letters (A, A′, A″), (B, B′, B″), etc. in the dispersion curves of Fig. 4. The intensity of the in-plane applied magnetic field is $H = 4$ kOe.

Therefore, the spin-wave dispersion curves were recalculated in the framework of dipole-exchange spin-wave theory by taking into account the hybridization between the three lowest-frequency modes [Fig. 4(b)]. Note that, in this case, a numerical calculation of $\nu_{nk}$ was required because the frequencies of the three modes (DE, 1-PSSW and 2-PSSW) were obtained as the eigenvalues of a $6 \times 6$ dynamical matrix with nonzero off-diagonal blocks. It has been found that the spin-wave hybridization is due to off-diagonal contributions of dipolar origin (i.e., the dimensionless factors $P_{nn'}$ and $Q_{nn'}$ with $n \neq n'$, defined by Eqs. (A1) and (A2) in Appendix A).

Comparing Figs. 4(a) and 4(b), it appears that the mode hybridization is crucial to obtaining a good agreement with the experimental results. In particular, we found that crossings of the different modes take place at values of $k$ in the range of $10^4$ rad/cm, where the dipole-dipole branch repulsion is so small that it causes the opening of tiny "gaps" in the spin-wave spectrum, hardly visible on the scale of Fig. 4. For larger values of $k$, instead, the dipolar interaction becomes so relevant that the modes repulsion reaches values of several GHz ($\Delta\nu \approx 5$ GHz for $k \approx 10^5$ rad/cm) and, as a consequence, the modes evolve keeping far apart from each other. Remarkably, the 1-PSSW mode assumes a negative slope to maximize the distance from the next PSSW one at large $k$ values. The modulus of the negative group velocity of the 1-PSSW mode can be estimated to be $v_g = 2\pi|\Delta\nu/\Delta k| \approx 2.2$ km/s, in the appropriate wave-vector range $(1.25 < k < 2.5) \times 10^5$ rad/cm, where the $\nu$ vs $k$ dispersion relation exhibits an almost linear behavior. In contrast, the DE mode exhibits a positive group velocity, whose value decreases from $v_g \approx 12.7$ km/s at $k \approx 0$ to $v_g \approx 0.6$ km/s for large wave-vector value. Remarkably, in the wave-vector range around $k \approx 1.0 \times 10^5$ rad/cm the two modes have a group velocity opposite in sign but equal in modulus, $v_g \approx 1.5$ km/s. A deeper insight into the behavior of the three lowest-energy spin-wave modes can be achieved looking at Fig. 5, where we show the spatial profile of $\mathbf{m}_k(x)$ calculated for selected values of the in-plane wave vector $k$, corresponding to relevant points of the calculated spin-wave dispersion [Fig. 4(b)]. In each panel the black line represents the distribution, across the film thickness ($0 < x/L < 1$), of the out-of-plane dynamic magnetization component $m_k^x(x)$, while the red line represents the in-plane one $m_k^z(x)$. For $k = 0$, the lowest frequency mode corresponds to the uniform mode (point A), while the other two modes are characterized by one node (point A′) and two nodes (point A″) across the thickness, as expected for the 1-PSSW and 2-PSSW modes, respectively. As the wave number $k$ is increased, the DE mode assumes the expected surface character (i.e., it localizes at $x = 0$), although its profile is somehow hybridized with that of the 1-PSSSW mode. In fact, the latter tends to localize, at large $k$ values, on the opposite film surface ($x = L$), reflecting mode repulsion and nonreciprocity opposite to that of the DE mode, as already put in evidence both in the experiment and in the micromagnetic simulations. Also the 2-PSSW mode, although preserving its oscillating behavior, tends to have a larger amplitude on the same film surface as the 1-PSSW mode.

The above behavior can be further explained observing the evolution as a function of $k$ of the diagonal dipolar factors

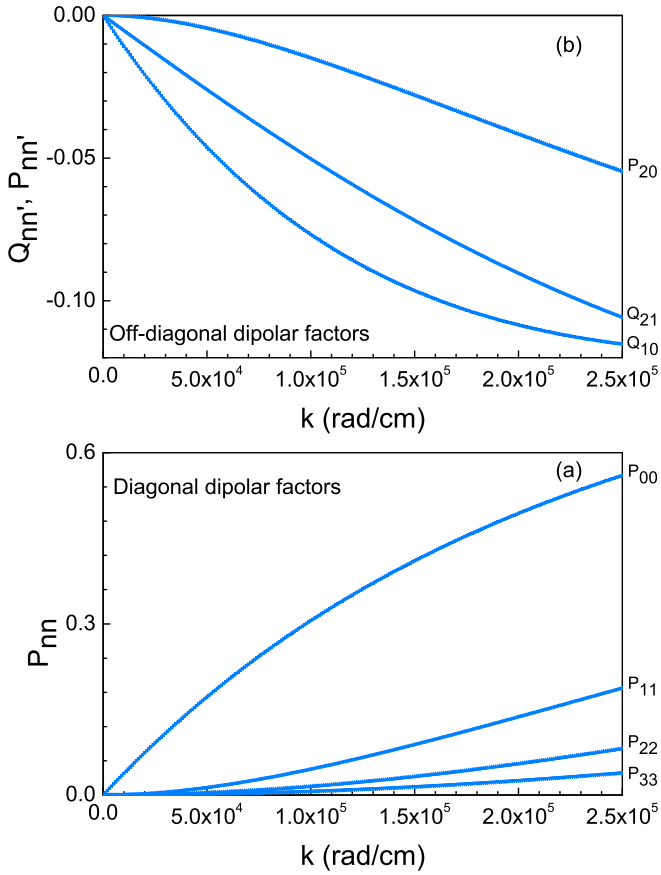


FIG. 6. Wave-vector dependence of the calculated diagonal (a) and off-diagonal (b) dimensionless dipolar factors, respectively defined in Eqs. (A1) and (A2) of Appendix A.

($P_{nn}$), and the off-diagonal ones ($P_{nn'}$ and $Q_{nn'}$ with $n \neq n'$), reported in Figs. 6(a) and 6(b), respectively, for the four lowest-frequency modes (corresponding to $n = 0, 1, 2, 3$). All the dimensionless dipolar factors increase in modulus with increasing the in-plane wave vector $k$. Moreover, at a fixed value of $k$ and of the mode index $n$, the diagonal and off-diagonal dipolar matrix elements turn out to be comparable in magnitude, thanks to the presence of a sizable perpendicular anisotropy and a large saturation magnetization. The latter, $M_s = 1700$ emu/cm$^3$ is more than one order of magnitude larger than in tangentially magnetized YIG films where, indeed, much smaller frequency gaps were found (e.g., for $k \approx 1 \times 10^5$ rad/cm, one has $\Delta\nu \approx 0.1$ GHz in the case of an in-plane saturated 495-nm-thick YIG film [30], to be compared with $\Delta\nu \approx 5$ GHz in the case of our Fe-N film). However, the magnitude of the off-diagonal elements decreases for the higher order modes, and this explains the fact that the behavior of the 3-PSSW mode is well described by the theory of independent modes. Instead, for the low-order modes, DE and 1-PSSW, the independent mode approach (where off-diagonal dipolar contributions are neglected) provides a quite good approximation only for small values of the in-plane wave vector $k$, whereas at values of $k > 10^5$ rad/cm, the modes hybridization turns out to be quite important. The consequent strong mode repulsion leads to a relatively large negative group velocity for the 1-PSSW mode, which is comparable in magnitude, even if opposite in sign, with respect to that of the DE mode. This means that, different from usual magnetic films, where all the modes have either positive or negative group velocity, depending on the choice of $\varphi = 90^\circ$ (MSSW geometry) or $\varphi = 0^\circ$ (Backward-wave geometry), respectively, here one could simultaneously excite two modes with opposite group velocity without changing the geometry. This could offer opportunities in magnon spintronics. For instance, one could explore the phenomena of a direct or reverse Doppler shift of spin waves, where the sign of the group velocity is a relevant parameter. When a spin wave interacts with an acoustic wave it can be considered as a moving Bragg grating, and a Doppler shift takes place in the experiments [31]. In particular, in order to fulfill the energy and momentum conservation laws, the spin wave undergoes a frequency shift equal to the frequency of the acoustic wave. However, if the group velocity of the spin wave is positive, one observes a regular Doppler effect, while if it is negative, the reverse Doppler effect is expected. The latter means that the frequency shift of the spin wave is positive on a copropagating acoustic wave, while it is negative on a counter-propagating acoustic wave.

## V. CONCLUSIONS

The spin-wave spectrum of an in-plane magnetized 78-nm-thick Fe-N film has been investigated by comparing Brillouin scattering experiments, micromagnetic simulations, and theoretical calculations of dipole-exchange spin-wave modes. Thanks to the presence of a marked perpendicular magnetic anisotropy and of a rather high saturation magnetization, the off-diagonal dipolar terms (which might be negligible in other systems, such as magnetically isotropic films with a low saturation magnetization and thickness in the $\mu$m range) become relevant as the wave number increases from $10^4$ to $10^5$ rad/cm. In this regime a strong hybridization between the DE and the 1-PSSW modes has been found. As a consequence, their crossing is avoided and one observes a very strong mode repulsion ($\Delta\nu \approx 5$ GHz for $k \approx 10^5$ rad/cm), with a negative group velocity for the lowest frequency mode. Moreover, in the wave-vector range of about $k \approx 1.0 \times 10^5$ rad/cm, the group velocity of the 1-PSSW mode assumes a value comparable to that of the DE one. The simultaneous presence of two modes with sizeable but opposite group velocity could offer opportunities in magnon spintronics, also considering the fact that FeN films can be prepared on substrates such as GaAs and Si and are, therefore, compatible with semiconductor components.

## ACKNOWLEDGMENTS

We thank F. Fortuna and L.-C. Garnier for ion implantation performed at CSNSM, Université Paris Sud-CNRS.

## APPENDIX A: EXPLICIT EXPRESSIONS FOR THE DIPOLAR FACTORS $P_{nn'}$ AND $Q_{nn'}$

In the case of totally unpinned spins on both film surfaces, the explicit expressions [21] for the dimensionless dipolar

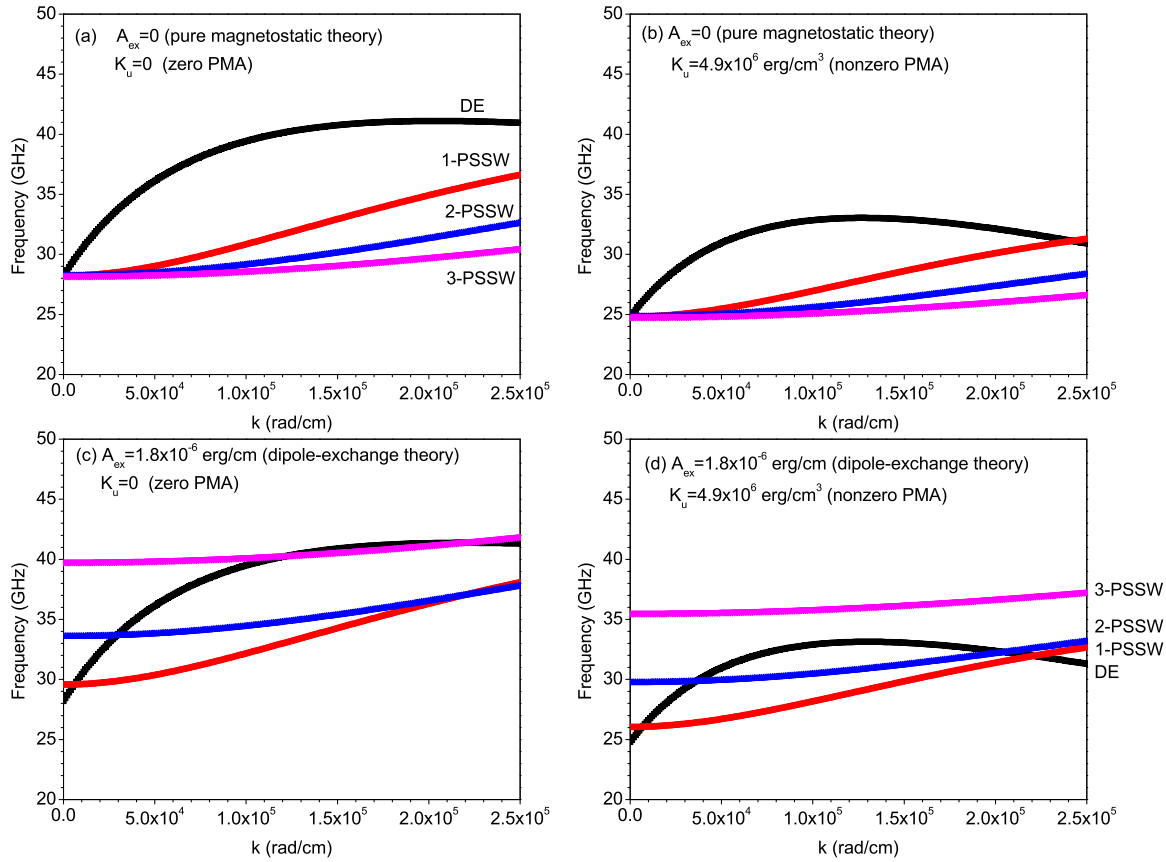


FIG. 7. Spin-wave dispersion relations of the four lowest-frequency independent spin-wave modes, calculated via the approximate analytic Eq. (B1) so as to show separately the effect of including the exchange coupling $A_{ex}$ and/or the out-of-plane uniaxial anisotropy $K_u$: (a) $A_{ex} = 0$, $K_u = 0$; (b) $A_{ex} = 0$, $K_u = 4.9 \times 10^6$ erg/cm$^3$; (c) $A_{ex} = 1.8 \times 10^{-6}$ erg/cm, $K_u = 0$; (d) $A_{ex} = 1.8 \times 10^{-6}$ erg/cm, $K_u = 4.9 \times 10^6$ erg/cm$^3$. In all four panels, the black line denotes the DE mode, the red line the 1-PSSW, the blue line the 2-PSSW, and the magenta line the 3-PSSW. The intensity of the in-plane applied magnetic field is $H = 4$ kOe.

factors $P_{nn'}$ and $Q_{nn'}$ are

$$P_{nn'} = \frac{k^2}{k_{n'}^2}\delta_{nn'} - \frac{k^4}{k_n^2 k_{n'}^2} F_n \frac{1}{\sqrt{(1+\delta_{0n})(1+\delta_{0n'})}} \times \left[\frac{1+(-1)^{n+n'}}{2}\right], \tag{A1}$$

$$Q_{nn'} = \frac{k^2}{k_{n'}^2}\left[\frac{\left(\frac{n'\pi}{L}\right)^2}{\left(\frac{n'\pi}{L}\right)^2 - \left(\frac{n\pi}{L}\right)^2}\frac{2}{kL} - \frac{k^2}{2k_n^2}F_n\right] \times \frac{1}{\sqrt{(1+\delta_{0n})(1+\delta_{0n'})}}\left[\frac{1-(-1)^{n+n'}}{2}\right], \tag{A2}$$

with $n, n' = 0, 1, 2, \cdots$ and

$$k_n^2 = k^2 + \left(\frac{n\pi}{L}\right)^2, \quad F_n = \frac{2}{kL}[1-(-1)^n e^{-kL}]. \tag{A3}$$

From (A1) it appears that $P_{n'n} = P_{nn'}$; moreover, one has $P_{n,n'} = 0$ if $n$ is even but $n'$ is odd (or *vice versa*). From (A2) it follows that $Q_{n'n} = -Q_{nn'}$; moreover, one has $Q_{n,n'} = 0$ if both $n$ and $n'$ are even (or both odd).

Finally, we quote the diagonal and off-diagonal dipole factors (together with their expansions in the limit $kL \ll 1$), which we exploited to calculate the hybridized spin-wave frequencies of the 78-nm Fe-N film reported in Fig. 4(b).

The lowest-order diagonal dipolar factors [plotted in Fig. 6(a)] are

$$P_{00} = 1 - \left(\frac{1-e^{-kL}}{kL}\right) \approx \frac{kL}{2}, \tag{A4}$$

$$P_{11} = \frac{k^2}{\left[k^2 + \left(\frac{\pi}{L}\right)^2\right]} - \frac{k^4}{\left[k^2 + \left(\frac{\pi}{L}\right)^2\right]^2}\left[2\left(\frac{1+e^{-kL}}{kL}\right)\right] \approx \left(\frac{kL}{\pi}\right)^2, \tag{A5}$$

$$P_{22} = \frac{k^2}{\left[k^2 + \left(\frac{2\pi}{L}\right)^2\right]} - \frac{k^4}{\left[k^2 + \left(\frac{2\pi}{L}\right)^2\right]^2}\left[2\left(\frac{1-e^{-kL}}{kL}\right)\right] \approx \left(\frac{kL}{2\pi}\right)^2, \tag{A6}$$

$$P_{33} = \frac{k^2}{\left[k^2 + \left(\frac{3\pi}{L}\right)^2\right]} - \frac{k^4}{\left[k^2 + \left(\frac{3\pi}{L}\right)^2\right]^2}\left[2\left(\frac{1+e^{-kL}}{kL}\right)\right] \approx \left(\frac{kL}{3\pi}\right)^2. \tag{A7}$$

The lowest-order off-diagonal dipolar factors [plotted in Fig. 6(b)] are

$$Q_{10} = -\frac{k^2}{\left[k^2 + \left(\frac{\pi}{L}\right)^2\right]}\left[\frac{\left(1+e^{-kL}\right)}{kL}\right]\frac{1}{\sqrt{2}} \approx -\sqrt{2}\frac{(kL)}{\pi^2}, \tag{A8}$$

$$Q_{21} = \frac{k^2}{\left[k^2+\left(\frac{\pi}{L}\right)^2\right]}\left[-\frac{1}{3}\frac{2}{kL} - \frac{k^2}{2\left[k^2+\left(\frac{2\pi}{L}\right)^2\right]}\left[2\left(\frac{1-e^{-kL}}{kL}\right)\right]\right] \approx -\frac{2}{3}\frac{(kL)}{\pi^2}, \tag{A9}$$

$$P_{02} = -\frac{k^2}{\left[k^2 + \left(\frac{2\pi}{L}\right)^2\right]}\left[2\left(\frac{1-e^{-kL}}{kL}\right)\right]\frac{1}{\sqrt{2}} \approx -\sqrt{2}\left(\frac{kL}{2\pi}\right)^2. \tag{A10}$$

## APPENDIX B: THE EFFECT OF EXCHANGE AND/OR ANISOTROPY ON THE SPIN-WAVE FREQUENCIES

In this Appendix, we explicitly calculate the frequencies of the independent spin-wave modes using the simple analytic form (10), obtained [20] imposing the vanishing of all the off-diagonal dipolar factors $P_{nn'}$ and $Q_{nn'}$ in the infinite dynamical matrix (9). Please note that in Eq. (10) one has $\Omega_{nk} = \omega_H + \omega_M\alpha[k^2 + (\frac{n\pi}{L})^2]$, $\omega_H = \gamma H$, $\omega_M = \gamma 4\pi M_s$, $\omega_U = \gamma\frac{2K_u}{M_s}$. The exchange parameter $\alpha = l_{ex}^2$ is related to the exchange length $l_{ex} = \sqrt{A_{ex}/K_d}$, where $A_{ex}$ is the exchange energy per unit length and $K_d = 2\pi M_s^2$ is the dipolar energy per unit volume. $H$ is the intensity of the external dc bias field, $4\pi M_s$ is the static dipolar field, and $2K_u/M_s$ is an effective static field associated with the out-of-plane magnetic anisotropy. Therefore, Eq. (10) can be rewritten in the equivalent form

$$\nu_{nk} = \frac{\gamma}{2\pi}\sqrt{H + \frac{2A_{ex}}{M_s}\left[k^2 + \left(\frac{n\pi}{L}\right)^2\right] + 4\pi M_s(1-P_{nn}) - \frac{2K_u}{M_s}} \times \sqrt{H + \frac{2A_{ex}}{M_s}\left[k^2 + \left(\frac{n\pi}{L}\right)^2\right] + 4\pi M_s P_{nn}\sin^2\varphi}. \tag{B1}$$

In Fig. 7, we report the dispersion curves of the four lowest-energy independent spin-wave modes, calculated using (B1), where in the MSSW configuration one has $\varphi = 90^\circ$, and $n = 0$, 1, 2, 3 correspond to the DE, 1-PSSW, 2-PSSW, and 3-PSSW modes, respectively. In order to unravel the influence of exchange and anisotropy on the spin-wave branches, the following cases were separately considered: (a) $A_{ex} = 0$, $K_u = 0$; (b) $A_{ex} = 0$, $K_u = 4.9 \times 10^6$ erg/cm$^3$; (c) $A_{ex} = 1.8 \times 10^{-6}$ erg/cm, $K_u = 0$; (d) $A_{ex} = 1.8 \times 10^{-6}$ erg/cm, $K_u = 4.9 \times 10^6$ erg/cm$^3$. It can be seen that the main effect of nonzero $A_{ex}$ is to remove the degeneracy, present at $k = 0$, of the volume magnetostatic modes through the out-of-plane exchange interaction (compare Figs. 7(a) and 7(c), or Figs. 7(b) and 7(d). The inclusion of a nonzero perpendicular magnetic anisotropy causes a frequency downshift of the dispersion branches (compare Figs. 7(a) and 7(b), or Figs. 7(c) and 7(d)) and a change of group velocity, which becomes negative at high $k$ for the DE branch. In this way, it appears clear that in the case of our 78-nm Fe-N film, both exchange and anisotropy concur to determine the crossing of the independent spin-wave branches at high wave vector ($k > 10^5$ rad/cm). Consequently, a repulsion between the spin-wave modes is expected, in the same $k$-range, when hybridization is taken into account. In Fig. 4 of the main text we have shown that this repulsion indeed takes place, and it is very strong owing to the $k$-dependence of the off-diagonal dimensionless dipolar factors $P_{nn'}$ and $Q_{nn'}$ with $n \neq n'$ (see Fig. 6).


[1] V. M. Agranovich and A. A. Maradudin, *Spin Waves and Magnetic Excitations* (North-Holland, Amsterdam, 1988).

[2] S. Neusser and D. Grundler, Adv. Mater. **21**, 2927 (2009).

[3] V. V. Kruglyak, S. O. Demokritov, and D. Grundler, J. Phys. D **43**, 264001 (2010).

[4] I. Žutić, J. Fabian, and S. Das Sarma, Rev. Mod. Phys. **76**, 323 (2004).

[5] A. V. Chumak, V. I. Vasuyuchka, A. A. Serga, and B. Hillebrands, Nat. Phys. **11**, 453 (2005).

[6] J. M. Owens, J. H. Collins, and R. L. Carter, Circuits Syst. Signal Process. **4**, 317 (1985).

[7] S. O. Demokritov, V. E. Demidov, O. Dzyapko, G. A. Melkov, A. A. Serga, B. Hillebrands, and A. N. Slavin, Nature **443**, 430 (2006).

[8] V. E. Demidov, O. Dzyapko, S. O. Demokritov, G. A. Melkov, and A. N. Slavin, Phys. Rev. Lett. **99**, 037205 (2007).

[9] M. Mohseni, R. Verba, T. Brächer, Q. Wang, D. A. Bozhko, B. Hillebrands, and P. Pirro, Phys. Rev. Lett. **122**, 197201 (2019).

[10] A. Navabi, C. Chen, A. Barra, M. Yazdani, G. Yu, M. Montazeri, M. Aldosary, J. Li, K. Wong, Q. Hu *et al.*, Phys. Rev. Applied **7**, 034027 (2017).

[11] G. Dieterle, J. Förster, H. Stoll, A. S. Semisalova, S. Finizio, A. Gangwar, M. Weigand, M. Noske, M. Fähnle, I. Bykova *et al.*, Phys. Rev. Lett. **122**, 117202 (2019).

[12] S. Klingler, V. Amin, S. Geprägs, K. Ganzhorn, H. Maier-Flaig, M. Althammer, H. Huebl, R. Gross, R. D. McMichael, M. D. Stiles *et al.*, Phys. Rev. Lett. **120**, 127201 (2018).

[13] K. An, V. S. Bhat, M. Mruczkiewicz, C. Dubs, and D. Grundler, Phys. Rev. Applied **11**, 034065 (2019).

[14] H. Qin, S. J. Hämäläinen, and S. van Dijken, Sci. Rep. **8**, 5755 (2018).

[15] T. Amarouche, L.-C. Garnier, M. Marangolo, M. Eddrief, V. H. Etgens, F. Fortuna, Y. Sadaoui, M. Tamine, J. L. Cantin, and H. J. von Bardeleben, J. Appl. Phys. **121**, 243903 (2017).

[16] L.-C. Garnier, M. Eddrief, S. Fin, D. Bisero, F. Fortuna, V. H. Etgens, and M. Marangolo, SPIN **06**, 1640014 (2016).

[17] I. S. Camara, S. Tacchi, L.-C. Garnier, M. Eddrief, F. Fortuna, G. Carlotti, and M. Marangolo, J. Phys. Condens. Matter **29**, 465803 (2017).

[18] S. Fin, R. Silvani, S. Tacchi, M. Marangolo, L.-C. Garnier, M. Eddrief, C. Hepburn, F. Fortuna, A. Rettori, M. G. Pini *et al.*, Sci. Rep. **8**, 9339 (2018).

[19] A. Vansteenkiste, J. Leliaert, M. Dvornik, M. Helsen, F. Garcia-Sanchez, and B. Van Waeyenberge, AIP Adv. **4**, 107133 (2014).
[20] B. A. Kalinikos, in *Linear and nonlinear spin waves in magnetic films and superlattices*, edited by M. G. Cottam (World Scientific, Singapore, 1994), pp. 89–156.
[21] B. A. Kalinikos and A. N. Slavin, J. Phys. C **19**, 7013 (1986).
[22] B. A. Kalinikos and N. V. Kozhus', Sov. Phys. Tech. Phys. **34**, 1105 (1989).
[23] B. A. Kalinikos, M. P. Kostylev, N. V. Kozhus', and A. N. Slavin, J. Phys.: Condens. Matter **2**, 9861 (1990).
[24] M. P. Kostylev, B. A. Kalinikos, and A. Dötsch, J. Magn. Magn. Mater. **145**, 93 (1995).
[25] L.-C. Garnier, Couches minces en Fe-N élaborées par implantation ionique : Propriétés structurales et magnétiques, Science des matériaux [cond-mat.mtrl-sci] (Université Paris-Saclay, 2019).
[26] G. Carlotti and G. Gubbiotti, Riv. Nuovo Cimento **22**, 1 (1999).
[27] B. Hillebrands, Rev. Sci. Instrum. **70**, 1589 (1999).
[28] R. E. Camley, P. Grünberg, and C. M. Mayr, Phys. Rev. B **26**, 2609 (1982).
[29] B. Hillebrands, Phys. Rev. B **41**, 530 (1990).
[30] A. Kreisel, F. Sauli, L. Bartosch, and P. Kopietz, Eur. Phys. J. B **71**, 59 (2009).
[31] A. V. Chumak, P. Dhagat, A. Jander, A. A. Serga, and B. Hillebrands, Phys. Rev. B **81**, 140404(R) (2010).